

Supporting Information

Wang et al. 10.1073/pnas.1216526110

SI Materials and Methods

Structure-Activity Relationship of Additional Compounds. Structure-activity relationship of additional compounds is shown in Table S1.

Chemistry. All chemicals were purchased from commercial vendors and used without further purification unless otherwise noted. ^1H and ^{13}C NMR spectra were recorded on a Bruker-300 NMR spectrometer. Chemical shifts are reported in parts per million referenced with respect to residual solvent, $\text{CD}_3\text{OD} = 3.31$ ppm and $\text{DMSO}-d_6 = 2.50$ ppm, or from internal standard, tetramethylsilane = 0.00 ppm. The following abbreviations were used in reporting spectra: singlet (s), doublet (d), triplet (t), quartet (q), multiplet (m), doublet of doublets (dd), and doublet of doublet of doublets (ddd). All reactions were carried out under N_2 atmosphere, unless otherwise stated. HPLC grade solvents were used for all the reactions. Flash column chromatography was performed using silica gel (230–400 mesh; Merck). Low-resolution mass spectra were obtained using an electrospray ionization (ESI) technique on a 3200 Q Trap LC tandem MS system (Applied Biosystems). The purity was assessed using a Shimadzu LC-MS system with a Waters XTerra MS C-18 column (part no. 186000538), 50×2.1 mm, at a flow rate of 0.3 mL/min; $\lambda = 250$ nm and 220 nm; mobile phase A, 0.1% formic acid in H_2O , and mobile phase B, 0.1% formic acid in 60% isopropanol, 30% CH_3CN , and 9.9% H_2O . The purified fractions were lyophilized. All compounds submitted for testing in a two-electrode voltage clamp (TEVC) assay and plaque reduction assay were confirmed to be >95.0% pure by LC-MS traces. All compounds were characterized by proton NMR, and selected compounds were also characterized by carbon NMR.

Synthesis of compounds with isoxazole, isoxazoline, and 1,2,4-oxadiazole headgroups. Compounds with the R group in the 5 position of isoxazole were synthesized starting from [3 + 2] cyclization of ethyl 2-chloro-2-(hydroxyimino)acetate with alkyne in the presence of triethylamine. The resulting ester was subsequently reduced by NaBH_4 , and the hydroxyl in the intermediate was then converted to a bromide-leaving group by PBr_3 ; this was followed by alkylation with amantadine to give the final product as shown in method I (Fig. S1A). Some of the compounds were synthesized alternatively from commercially available chloride and aldehyde intermediates by alkylation and reductive amination as shown in method II and method III, respectively (Fig. S1A). Compounds with the R group in the 3 position of isoxazole and isoxazoline were synthesized starting from [3 + 2] cyclization of in situ-generated nitron with propargyl bromide or allyl bromide (method IV), followed by alkylation (Fig. S1B). Compounds with the R group in the 3 or 5 position of 1,2,4-oxadiazole were synthesized from commercially available chloride intermediates (Fig. S1C). Details about the synthesis procedure are provided in the next sections.

General procedure for the synthesis of isoxazole compounds in method I. Alkyne (1 eq) and ethyl 2-chloro-2-(hydroxyimino)acetate (1.5 eq) were dissolved in THF. The solution was cooled down to 0 °C in an ice bath. Triethylamine (3 eq) was added drop-wise over 30 min. The mixture was then warmed to room temperature and stirred overnight. Solvent was removed under reduced pressure, and the resulting residue was extracted with ethyl acetate and water. The organic layers were combined, dried over anhydrous magnesium sulfate, filtered, and concentrated under reduced pressure. The crude product was purified by silica gel flash column chromatography to give the isoxazole ester (10–30% ethyl acetate/hexane). The isoxazole ester was subsequently reduced using NaBH_4 (5 eq) in CH_3OH at room temperature overnight. Diluted HCl was added,

and the reaction mixture was concentrated under reduced pressure. The resulting residue was extracted with ethyl acetate and water. The organic layers were combined, dried over anhydrous magnesium sulfate, filtered, and concentrated under reduced pressure. The crude product proceeded to the next step of bromination without further purification. The hydroxyl isoxazole intermediate was then brominated using PBr_3 in anhydrous CH_2Cl_2 . Briefly, PBr_3 (1 eq) was added drop-wise to a solution of hydroxyl isoxazole in anhydrous CH_2Cl_2 at 0 °C. The mixture was kept at the same temperature for 30 min, and solvent was then removed under reduced pressure. Ethyl acetate was added and extracted with water three times. The organic layer was separated, dried over anhydrous magnesium sulfate, filtered, and concentrated under reduced pressure. The crude product proceeded to next step, alkylation with amantadine, according to the following general procedure as described for method II.

General procedure for the alkylation of isoxazole/oxadiazole chloride/bromide with amantadine/1-amino-3-adamantol in method II. The chloride/bromide (1 eq) and amantadine (1.5 eq) were dissolved in isopropanol, and CsI (0.1 eq) and triethylamine (2 eq) were then added. The reaction mixture was heated to reflux overnight. The solvent was removed under reduced pressure, and the resulting residue was extracted with ethyl acetate and water. The organic layer was separated, dried over anhydrous magnesium sulfate, filtered, and concentrated under reduced pressure. The mixture was then purified by silica gel flash column chromatography to give the final product (5–10% $\text{CH}_3\text{OH}/\text{CH}_2\text{Cl}_2$).

General procedure for the reductive amination with amantadine in method III. Adamantane (1 eq) and aldehyde (1 eq) were mixed, and 2 mL of titanium (IV) isopropoxide was added. The resulting slurry was heated to 100 °C and stirred overnight. The solution was then cooled down to 0 °C in an ice bath, methanol was added, and sodium borohydride (4 eq) was added portion-wise over 10 min. The solution was warmed to room temperature and stirred overnight. The solvent was removed under reduced pressure, and the resulting residue was extracted with ethyl acetate and water. The organic layer was separated, dried over anhydrous magnesium sulfate, filtered, and concentrated under reduced pressure. The mixture was then purified by silica gel flash column chromatography to give the final product (5–10% $\text{CH}_3\text{OH}/\text{CH}_2\text{Cl}_2$).

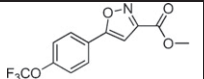
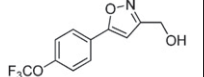
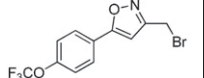
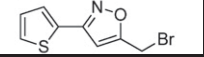
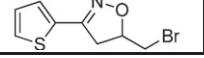
General procedure for the synthesis of isoxazole and isoxazoline in method IV. Oximes were prepared according to a previously published procedure (1). To a cooled solution (0 °C using an ice bath) of oximes (1 eq), propargyl bromide/allyl bromide (1.2 eq) and triethylamine (1 eq) in CH_2Cl_2 were added drop-wise to 8% aqueous sodium hypochlorite. After addition, the solution was warmed to room temperature and stirred overnight. The mixture was separated, and the aqueous layer was extracted with CH_2Cl_2 twice. The organic layers were combined, dried over anhydrous magnesium sulfate, filtered, and concentrated under reduced pressure. The mixture was then purified by silica gel flash column chromatography to give the intermediate (10–40% ethyl acetate/hexane). The next step, alkylation, was performed according to the general procedure as described for method II.

The following compound was synthesized using method I: **M2WJ446**.

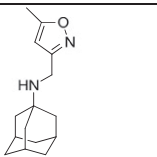
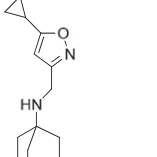
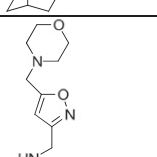
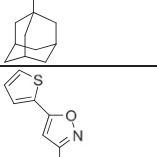
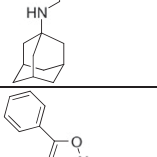
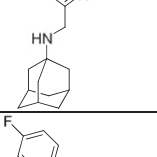
The following compounds were synthesized using method II: **M2WJ363, M2WJ376, M2WJ377, M2WJ378, M2WJ379, M2WJ380, M2WJ381, M2WJ386, M2WJ388, M2WJ389, M2WJ393, M2WJ396, M2WJ397, M2WJ398, M2WJ399, M2WJ400, M2WJ401, M2WJ403, M2WJ405, M2WJ406, M2WJ408, M2WJ409, M2WJ423, M2WJ430, and M2WJ434**.

The following compounds were synthesized using method III: **M2WJ332, M2WJ352, M2WJ353, M2WJ358, M2WJ361, M2WJ366, M2WJ367, M2WJ368, M2WJ369, M2WJ370, and M2WJ371**.

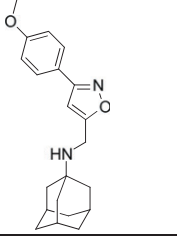
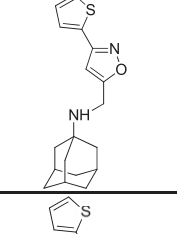
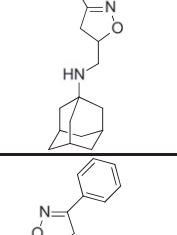
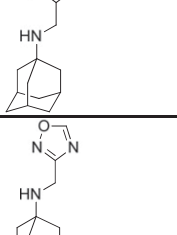
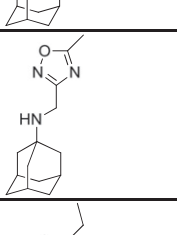
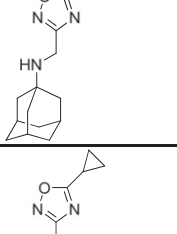
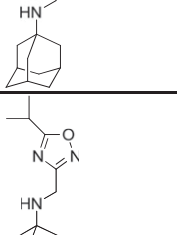

Characterization of intermediates is illustrated in the following chart:

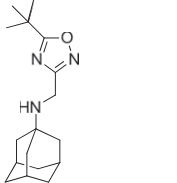
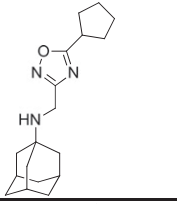
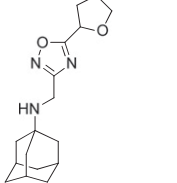
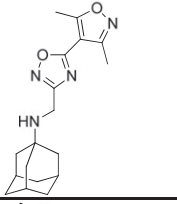
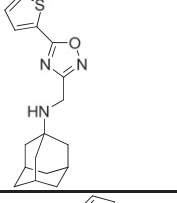
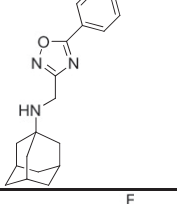
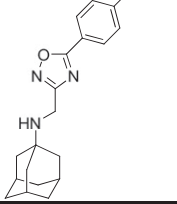
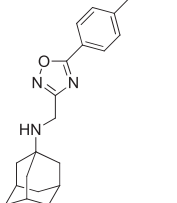
	Methyl 5-(4-(trifluoromethoxy)phenyl)isoxazole-3-carboxylate. ¹ HNMR (300 MHz, CDCl ₃): δ 7.86 (d, <i>J</i> = 8.67 Hz, 2H), 7.35 (d, <i>J</i> = 8.67 Hz, 2H), 6.95 (s, 1H), 4.02 (s, 3H).
	(5-(4-(trifluoromethoxy)phenyl)isoxazol-3-yl)methanol. ¹ HNMR (300 MHz, CDCl ₃): δ 7.76 (d, <i>J</i> = 8.97 Hz, 2H), 7.29 (d, <i>J</i> = 8.67 Hz, 2H), 6.59 (s, 1H), 4.81 (s, 2H), 2.86 (s, 1H). ¹⁹ FNMR (300 MHz, CDCl ₃): δ -57.78.
	3-(bromomethyl)-5-(4-(trifluoromethoxy)phenyl)isoxazole. ¹ HNMR (300 MHz, CDCl ₃): δ 7.83 (d, <i>J</i> = 8.76 Hz, 2H), 7.33 (d, <i>J</i> = 8.76 Hz, 2H), 6.63 (s, 1H), 4.48 (s, 2H). ¹⁹ FNMR (300 MHz, CDCl ₃): δ -57.72.
	5-(bromomethyl)-3-(thiophen-2-yl)isoxazole. ¹ HNMR (300 MHz, CDCl ₃): δ 7.52–7.50 (m, 1H), 7.30–7.28 (m, 1H), 7.16–7.13 (m, 1H), 6.47 (s, 1H), 4.45 (s, 2H).
	5-(bromomethyl)-3-(thiophen-2-yl)-4,5-dihydroisoxazole. ¹ HNMR (300 MHz, CDCl ₃): δ 7.50–7.48 (m, 1H), 7.31–7.29 (m, 1H), 7.17–7.14 (m, 1H), 5.07–5.02 (m, 1H), 3.75–3.48 (m, 3H), 3.47–3.25 (m, 1H).

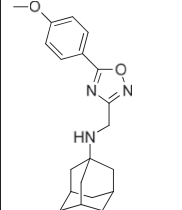
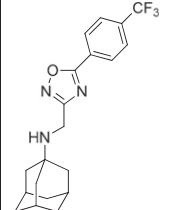
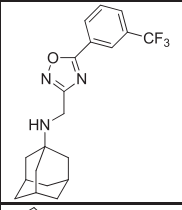
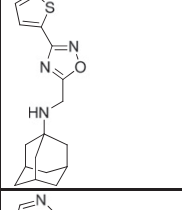
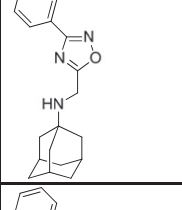
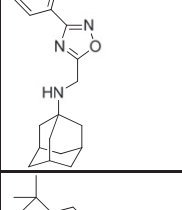
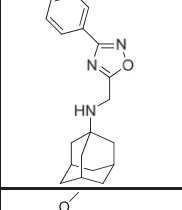
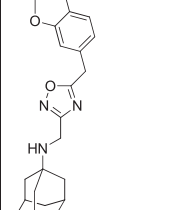
Characterization of final products is illustrated in the following chart:

	N-((5-methylisoxazol-3-yl)methyl)adamantan-1-amine (M2WJ369). ¹ HNMR (300 MHz, CD ₃ OD): δ 6.19 (s, 1H), 3.77 (s, 2H), 2.40 (s, 3H), 2.09–2.07 (m, 3H), 1.73–1.69 (m, 12H). ¹³ CNMR (75 MHz, CD ₃ OD): 171.11, 164.84, 102.39, 52.28, 42.78, 37.63, 37.08, 30.99, 11.98. ESI-MS: <i>m/z</i> (M + H ⁺): 247.4 (calculated), 247.4 (found).
	N-((5-cyclopropylisoxazol-3-yl)methyl)adamantan-1-amine (M2WJ379). ¹ HNMR (300 MHz, CD ₃ OD): δ 6.12 (s, 1H), 2.08 (s, 2H), 2.08–2.01 (m, 4H), 1.59–1.52 (m, 12H), 1.03–0.99 (m, 2H), 0.84–0.80 (m, 2H). ESI-MS: <i>m/z</i> (M + H ⁺): 272.4 (calculated), 272.4 (found).
	N-((5-(morpholinomethyl)isoxazol-3-yl)methyl)adamantan-1-amine (M2WJ371). ¹ HNMR (300 MHz, CD ₃ OD- <i>d</i> ₆): δ 6.43 (s, 1H), 3.82 (s, 2H), 3.71 (s, 2H), 3.69 (t, <i>J</i> = 4.68 Hz, 4H), 2.53 (t, <i>J</i> = 4.68 Hz, 4H), 2.10–2.07 (m, 3H), 1.74–1.69 (m, 12H). ESI-MS: <i>m/z</i> (M + H ⁺): 332.5 (calculated), 332.5 (found).
	N-((5-(thiophen-2-yl)isoxazol-3-yl)methyl)adamantan-1-amine (M2WJ332). ¹ HNMR (300 MHz, DMSO- <i>d</i> ₆): δ 7.83 (d, <i>J</i> = 4.59 Hz, 1H), 7.72 (d, <i>J</i> = 4.59 Hz, 1H), 7.26 (dd, <i>J</i> = 4.82 Hz, 3.84 Hz, 1H), 6.85 (s, 1H), 3.78 (s, 2H), 2.08–2.05 (m, 3H), 1.65–1.63 (m, 12H). ESI-MS: <i>m/z</i> (M + H ⁺): 315.5 (calculated), 315.1 (found).
	N-((5-phenylisoxazol-3-yl)methyl)adamantan-1-amine (M2WJ352). ¹ HNMR (300 MHz, DMSO- <i>d</i> ₆): δ 7.90–7.87 (m, 2H), 7.56–7.53 (m, 3H), 7.02 (s, 1H), 3.80 (s, 2H), 2.07–2.05 (m, 3H), 1.66–1.64 (m, 12H). ESI-MS: <i>m/z</i> (M + H ⁺): 309.4 (calculated), 309.3 (found).
	N-((5-(4-fluorophenyl)isoxazol-3-yl)methyl)adamantan-1-amine (M2WJ366). ¹ HNMR (300 MHz, DMSO- <i>d</i> ₆): δ 7.92 (dd, <i>J</i> = 8.21 Hz, 6.27 Hz, 2H), 7.36 (dd, <i>J</i> = 5.79 Hz, 2.73 Hz, 2H), 6.97 (s, 1H), 3.75 (s, 2H), 2.02–2.00 (m, 3H), 1.63–1.61 (m, 12H). ESI-MS: <i>m/z</i> (M + H ⁺): 327.4 (calculated), 327.2 (found).

	N-((5-(4-chlorophenyl)isoxazol-3-yl)methyl)adamantan-1-amine (M2WJ367). ¹ HNMR (300 MHz, CD ₃ OD): δ 7.82–7.78 (m, 2H), 7.53–7.49 (m, 2H), 6.84 (s, 1H), 3.86 (s, 2H), 2.10–2.08 (m, 3H), 1.75–1.71 (m, 12H). ¹³ CNMR (75 MHz, CD ₃ OD): 169.98, 165.58, 137.26, 130.43, 128.25, 127.40, 100.97, 52.37, 42.82, 37.62, 37.15, 30.99. ESI-MS: <i>m/z</i> (M + H ⁺): 343.9 (calculated), 343.4 (found).
	N-((5-(4-bromophenyl)isoxazol-3-yl)methyl)adamantan-1-amine (M2WJ370). ¹ HNMR (300 MHz, CD ₃ OD): δ 7.76–7.66 (m, 4H), 6.86 (s, 1H), 3.87 (s, 2H), 2.10–2.08 (m, 2H), 1.77–1.73 (m, 12H). ESI-MS: <i>m/z</i> (M + H ⁺): 388.3 (calculated), 388.1 (found).
	N-((5-(p-tolyl)isoxazol-3-yl)methyl)adamantan-1-amine (M2WJ368). ¹ HNMR (300 MHz, DMSO- <i>d</i> ₆): δ 7.73 (d, <i>J</i> = 8.1 Hz, 2H), 7.33 (d, <i>J</i> = 8.1 Hz, 2H), 6.90 (s, 1H), 3.75 (s, 2H), 2.36 (s, 3H), 2.02–2.00 (m, 3H), 1.63–1.60 (m, 12H). ESI-MS: <i>m/z</i> (M + H ⁺): 323.4 (calculated), 323.4 (found).
	N-((5-(4-methoxyphenyl)isoxazol-3-yl)methyl)adamantan-1-amine (M2WJ358). ¹ HNMR (300 MHz, CD ₃ OD): δ 7.76–7.73 (m, 2H), 7.05–7.02 (m, 2H), 6.67 (s, 1H), 3.84 (s, 2H), 3.83 (s, 2H), 2.09–2.07 (m, 3H), 1.76–1.72 (m, 12H). ¹³ CNMR (75 MHz, CD ₃ OD): 171.31, 165.34, 162.82, 128.37, 121.39, 115.54, 98.97, 55.89, 52.36, 42.80, 37.63, 37.16, 30.99. ESI-MS: <i>m/z</i> (M + H ⁺): 339.4 (calculated), 339.4 (found).
	N-((5-(4-(trifluoromethoxy)phenyl)isoxazol-3-yl)methyl)adamantan-1-amine (M2WJ446). ¹ HNMR (300 MHz, CD ₃ OD): δ 7.93 (d, <i>J</i> = 8.85 Hz, 2H), 7.42 (d, <i>J</i> = 8.85 Hz, 2H), 6.88 (s, 1H), 3.89 (s, 2H), 2.12–2.09 (m, 3H), 1.78–1.71 (m, 12H). ESI-MS: <i>m/z</i> (M + H ⁺): 393.4 (calculated), 393.4 (found).
	N-((3-(pyridin-3-yl)isoxazol-5-yl)methyl)adamantan-1-amine (M2WJ380). ¹ HNMR (300 MHz, CD ₃ OD): δ 9.01–8.99 (m, 1H), 8.64–8.62 (m, 1H), 8.30–8.26 (m, 1H), 7.58–7.54 (m, 1H), 6.86 (s, 1H), 3.98 (s, 2H), 2.10–2.08 (m, 3H), 1.76–1.70 (m, 12H). ESI-MS: <i>m/z</i> (M + H ⁺): 310.4 (calculated), 310.3 (found).
	N-((3-phenylisoxazol-5-yl)methyl)adamantan-1-amine (M2WJ353). ¹ HNMR (300 MHz, DMSO- <i>d</i> ₆): δ 7.90–7.87 (m, 2H), 7.55–7.52 (m, 3H), 6.88 (s, 1H), 3.89 (s, 2H), 2.06–2.04 (m, 3H), 1.67–1.63 (m, 12H). ESI-MS: <i>m/z</i> (M + H ⁺): 309.4 (calculated), 309.4 (found).
	N-((3-(4-bromophenyl)isoxazol-5-yl)methyl)adamantan-1-amine (M2WJ361). ¹ HNMR (300 MHz, CD ₃ OD): δ 7.77–7.73 (m, 2H), 7.66–7.63 (m, 2H), 3.94 (s, 2H), 2.10–2.08 (m, 3H), 1.75–1.70 (m, 12H). ESI-MS: <i>m/z</i> (M + H ⁺): 388.3 (calculated), 388.3 (found).

	N-((3-(4-methoxyphenyl)isoxazol-5-yl)methyl)adamantan-1-amine (M2WJ386). ^1H NMR (300 MHz, DMSO- d_6): δ 7.78 (d, J = 8.73 Hz, 2H), 7.06 (d, J = 8.73 Hz, 2H), 6.82 (s, 1H), 3.81 (s, 3H), 3.73 (s, 2H), 2.10–2.08 (m, 3H), 1.64–1.60 (m, 12H). ESI-MS: m/z ($M + H^+$): 339.4 (calculated), 339.2 (found).
	N-((3-(thiophen-2-yl)isoxazol-5-yl)methyl)adamantan-1-amine (M2WJ372). ^1H NMR (300 MHz, DMSO- d_6): δ 7.80–7.77 (m, 2H), 7.26–7.23 (m, 1H), 7.16 (s, 1H), 4.48 (s, 2H), 2.17–2.15 (m, 3H), 1.92–1.88 (m, 6H), 1.71–1.69 (m, 6H). ESI-MS: m/z ($M + H^+$): 315.5 (calculated), 315.6 (found).
	N-((3-(thiophen-2-yl)-4,5-dihydroisoxazol-5-yl)methyl)adamantan-1-amine (M2WJ373). ^1H NMR (300 MHz, CD_3OD): δ 7.53 (dd, J = 5.10 Hz, 1.08 Hz, 1H), 7.32 (dd, J = 3.66 Hz, 1.08 Hz, 1H), 7.10 (dd, J = 5.10 Hz, 3.66 Hz, 1H), 4.87–4.75 (m, 1H), 3.52 (dd, J = 16.80 Hz, 10.35 Hz, 1H), 3.20 (dd, J = 16.80 Hz, 7.29 Hz, 1H), 2.80 (ddd, J = 23.64 Hz, 12.09 Hz, 7.80 Hz, 1H), 2.09–2.06 (m, 3H), 1.74–1.64 (m, 12H). ESI-MS: m/z ($M + H^+$): 317.5 (calculated), 317.5 (found).
	N-((3-phenyl-4,5-dihydroisoxazol-5-yl)methyl)adamantan-1-amine (M2WJ388). ^1H NMR (300 MHz, CD_3OD): δ 7.70–7.67 (m, 2H), 7.44–7.42 (m, 3H), 4.87–4.76 (m, 1H), 3.51 (dd, J = 17.01 Hz, 10.47 Hz, 1H), 3.18 (dd, J = 17.01 Hz, 7.32 Hz, 1H), 2.80 (ddd, J = 27.93 Hz, 12.00 Hz, 7.83 Hz, 1H), 2.08–2.06 (m, 3H), 1.71–1.68 (m, 12H). ESI-MS: m/z ($M + H^+$): 311.4 (calculated), 311.4 (found).
	N-((1,2,4-oxadiazol-3-yl)methyl)adamantan-1-amine (M2WJ396). ^1H NMR (300 MHz, CD_3OD): δ 9.19 (s, 1H), 3.95 (s, 2H), 2.10–2.08 (m, 3H), 1.75–1.72 (m, 12H). ESI-MS: m/z ($M + H^+$): 234.3 (calculated), 234.3 (found).
	N-((5-methyl-1,2,4-oxadiazol-3-yl)methyl)adamantan-1-amine (M2WJ405). ^1H NMR (300 MHz, CD_3OD): δ 3.85 (s, 2H), 2.58 (s, 3H), 2.10–2.08 (m, 3H), 1.76–1.66 (m, 12H). ESI-MS: m/z ($M + H^+$): 248.3 (calculated), 248.4 (found).
	N-((5-ethyl-1,2,4-oxadiazol-3-yl)methyl)adamantan-1-amine (M2WJ408). ^1H NMR (300 MHz, CD_3OD): δ 3.86 (s, 2H), 2.93 (q, J = 7.62 Hz, 2H), 2.10–2.08 (m, 3H), 1.76–1.66 (m, 12H), 1.37 (t, J = 7.62 Hz, 3H). ESI-MS: m/z ($M + H^+$): 262.3 (calculated), 262.1 (found).
	N-((5-cyclopropyl-1,2,4-oxadiazol-3-yl)methyl)adamantan-1-amine (M2WJ409). ^1H NMR (300 MHz, CD_3OD): δ 3.81 (s, 2H), 2.30–2.22 (m, 1H), 2.16–2.10 (m, 3H), 1.80–1.60 (m, 12H), 1.35–1.21 (m, 2H), 1.18–1.08 (m, 2H). ESI-MS: m/z ($M + H^+$): 274.4 (calculated), 274.1 (found).
	N-((5-isopropyl-1,2,4-oxadiazol-3-yl)methyl)adamantan-1-amine (M2WJ400). ^1H NMR (300 MHz, CD_3OD): δ 3.24 (q, J = 6.99 Hz, 1H), 2.10–2.08 (m, 3H), 1.76–1.66 (m, 12H), 1.38 (d, J = 6.99 Hz, 6H). ESI-MS: m/z ($M + H^+$): 276.4 (calculated), 276.1 (found).

	N-((5-(tert-butyl)-1,2,4-oxadiazol-3-yl)methyl)adamantan-1-amine (M2WJ401). ¹ HNMR (300 MHz, CD ₃ OD): δ 3.86 (s, 2H), 2.10–2.08 (m, 3H), 1.76–1.66 (m, 12H), 1.47 (s, 9H). ESI-MS: <i>m/z</i> (M + H ⁺): 290.4 (calculated), 290.2 (found).
	N-((5-cyclopentyl-1,2,4-oxadiazol-3-yl)methyl)adamantan-1-amine (M2WJ403). ¹ HNMR (300 MHz, CD ₃ OD): δ 3.86 (s, 2H), 3.45–3.30 (m, 1H), 2.25–2.02 (m, 5H), 1.98–1.62 (m, 18H). ESI-MS: <i>m/z</i> (M + H ⁺): 302.4 (calculated), 302.1 (found).
	N-((5-(tetrahydrofuran-2-yl)-1,2,4-oxadiazol-3-yl)methyl)adamantan-1-amine (M2WJ423). ¹ HNMR (300 MHz, CD ₃ OD): δ 5.23–5.19 (m, 1H), 4.12–3.96 (m, 2H), 3.90 (s, 2H), 2.42–2.37 (m, 1H), 2.26–2.24 (m, 1H), 2.13–2.07 (m, 5H), 1.81–1.70 (m, 12H). ESI-MS: <i>m/z</i> (M + H ⁺): 304.4 (calculated), 304.4 (found).
	N-((5-(3,5-dimethylisoxazol-4-yl)-1,2,4-oxadiazol-3-yl)methyl)adamantan-1-amine (M2WJ430). ¹ HNMR (300 MHz, CD ₃ OD): δ 3.95 (s, 2H), 2.79 (s, 3H), 2.54 (s, 3H), 2.12–2.08 (m, 3H), 1.76–1.66 (m, 12H). ¹³ CNMR (75 MHz, CD ₃ OD): 175.00, 171.09, 160.04, 104.59, 52.38, 42.81, 37.59, 37.07, 31.00, 13.09, 11.63. ESI-MS: <i>m/z</i> (M + H ⁺): 329.4 (calculated), 329.5 (found).
	N-((5-(thiophen-2-yl)-1,2,4-oxadiazol-3-yl)methyl)adamantan-1-amine (M2WJ389). ¹ HNMR (300 MHz, CD ₃ OD): δ 7.96 (dd, <i>J</i> = 3.81 Hz, 1.17 Hz, 1H), 7.88 (dd, <i>J</i> = 5.01 Hz, 1.14 Hz, 1H), 7.28 (dd, <i>J</i> = 5.04 Hz, 3.84 Hz, 1H), 3.93 (s, 2H), 2.10–2.08 (m, 3H), 1.76–1.68 (m, 12H). ESI-MS: <i>m/z</i> (M + H ⁺): 316.4 (calculated), 316.2 (found).
	N-((5-phenyl-1,2,4-oxadiazol-3-yl)methyl)adamantan-1-amine (M2WJ399). ¹ HNMR (300 MHz, CD ₃ OD): δ 8.17–8.13 (m, 2H), 7.69–7.57 (m, 3H), 3.96 (s, 2H), 2.11–2.08 (m, 3H), 1.78–1.70 (m, 12H). ESI-MS: <i>m/z</i> (M + H ⁺): 310.4 (calculated), 310.4 (found).
	N-((5-(4-fluorophenyl)-1,2,4-oxadiazol-3-yl)methyl)adamantan-1-amine (M2WJ406). ¹ HNMR (300 MHz, CD ₃ OD): δ 8.23–8.19 (m, 2H), 7.38–7.32 (m, 2H), 3.95 (s, 2H), 2.11–2.08 (m, 3H), 1.77–1.67 (m, 12H). ESI-MS: <i>m/z</i> (M + H ⁺): 328.4 (calculated), 328.1 (found).
	N-((5-(p-tolyl)-1,2,4-oxadiazol-3-yl)methyl)adamantan-1-amine (M2WJ393). ¹ HNMR (300 MHz, CD ₃ OD): δ 8.03 (d, <i>J</i> = 8.25 Hz, 2H), 7.41 (d, <i>J</i> = 8.25 Hz, 2H), 3.94 (s, 2H), 2.45 (s, 3H), 2.11–2.09 (m, 3H), 1.77–1.70 (m, 12H). ESI-MS: <i>m/z</i> (M + H ⁺): 324.4 (calculated), 324.3 (found).

	N-((5-(4-methoxyphenyl)-1,2,4-oxadiazol-3-yl)methyl)adamantan-1-amine (M2WJ378). ^1H NMR (300 MHz, $\text{DMSO}-d_6$): δ 8.03 (d, J = 8.82 Hz, 2H), 7.15 (d, J = 8.82 Hz, 2H), 3.86 (s, 3H), 3.83 (s, 2H), 2.11–2.08 (m, 3H), 1.65–1.58 (m, 12H). ESI-MS: m/z ($M + H^+$): 340.4 (calculated), 340.4 (found).
	N-((5-(4-(trifluoromethyl)phenyl)-1,2,4-oxadiazol-3-yl)methyl)adamantan-1-amine (M2WJ397). ^1H NMR (300 MHz, CD_3OD): δ 8.35 (d, J = 8.55 Hz, 2H), 7.93 (d, J = 8.55 Hz, 2H), 3.99 (s, 2H), 2.11–2.08 (m, 3H), 1.78–1.71 (m, 12H). ESI-MS: m/z ($M + H^+$): 378.4 (calculated), 378.4 (found).
	N-((5-(3-(trifluoromethyl)phenyl)-1,2,4-oxadiazol-3-yl)methyl)adamantan-1-amine (M2WJ398). ^1H NMR (300 MHz, CD_3OD): δ 8.43–8.40 (m, 2H), 8.00–7.97 (m, 1H), 7.86–7.80 (m, 1H), 3.99 (s, 2H), 2.11–2.08 (m, 3H), 1.79–1.72 (m, 12H). ESI-MS: m/z ($M + H^+$): 378.4 (calculated), 378.4 (found).
	N-((3-(thiophen-2-yl)-1,2,4-oxadiazol-5-yl)methyl)adamantan-1-amine (M2WJ363). ^1H NMR (300 MHz, $\text{DMSO}-d_6$): δ 7.90–7.86 (m, 1H), 7.82–7.78 (m, 1H), 7.27–7.24 (m, 1H), 4.03 (s, 2H), 2.02–2.00 (m, 3H), 1.59–1.50 (m, 12H). ESI-MS: m/z ($M + H^+$): 316.4 (calculated), 316.4 (found).
	N-((3-(pyridin-3-yl)-1,2,4-oxadiazol-5-yl)methyl)adamantan-1-amine (M2WJ381). ^1H NMR (300 MHz, $\text{DMSO}-d_6$): δ 9.18–9.16 (m, 1H), 8.79–8.77 (m, 1H), 8.38–8.36 (m, 1H), 7.64–7.62 (m, 1H), 4.09 (s, 2H), 2.07–2.04 (m, 3H), 1.62–1.55 (m, 12H). ESI-MS: m/z ($M + H^+$): 311.4 (calculated), 311.5 (found).
	N-((3-phenyl-1,2,4-oxadiazol-5-yl)methyl)adamantan-1-amine (M2WJ376). ^1H NMR (300 MHz, $\text{DMSO}-d_6$): δ 8.02–7.99 (m, 2H), 7.58–7.56 (m, 3H), 4.06 (s, 2H), 2.02–2.00 (m, 3H), 1.62–1.55 (m, 12H). ESI-MS: m/z ($M + H^+$): 310.4 (calculated), 310.6 (found).
	N-((3-(4-(tert-butyl)phenyl)-1,2,4-oxadiazol-5-yl)methyl)adamantan-1-amine (M2WJ377). ^1H NMR (300 MHz, $\text{DMSO}-d_6$): δ 7.92 (d, J = 8.43 Hz, 2H), 7.57 (d, J = 8.43 Hz, 2H), 4.05 (s, 2H), 2.02–2.00 (m, 3H), 1.59–1.52 (m, 12H), 1.31 (s, 9H). ESI-MS: m/z ($M + H^+$): 366.5 (calculated), 366.3 (found).
	N-((5-(3,4-dimethoxybenzyl)-1,2,4-oxadiazol-3-yl)methyl)adamantan-1-amine (M2WJ434). ^1H NMR (300 MHz, CD_3OD): δ 6.95–6.89 (m, 3H), 4.22 (s, 2H), 3.85 (s, 2H), 3.82 (s, 3H), 3.81 (s, 3H), 2.09–2.06 (m, 3H), 1.72–1.67 (m, 12H). ESI-MS: m/z ($M + H^+$): 384.5 (calculated), 384.4 (found).

The following compounds were synthesized using method IV: M2WJ372 and M2WJ373.

Equations Used to Fit the IC₅₀ in the TEVC Assay. Typically, IC₅₀ values were obtained as described previously, by fitting to the Hill equation. However, measurements in triplicate for multiple concentrations of compound were not practical due to the large amount of time required to make the electrophysiological recordings. Therefore, for many weakly active compounds, we measured the inhibition in triplicate at only 100 μM. To relate the degree of inhibition at 100 μM to the IC₅₀, we created a calibration curve of a series of compounds whose IC₅₀ had been determined previously (method A). A plot of percent inhibition at 100 μM vs. IC₅₀ for these compounds (Fig. S2 A and B) was analyzed using nonlinear least squares fitting to the equation:

$$IC_{50} = \frac{[\text{inhibitor}][M2]}{[\text{inhibitor}M2]} = 100 \left(\frac{100-f}{f} \right)^n.$$

The best-fit exponential (n) was 0.99. This equation provides a good estimate of the IC₅₀ when the degree of inhibition is up to ~70–80%. As the fractional inhibition becomes higher, small errors in the degree of inhibition (typically 3–5% in our assay) cause large errors in the predicted IC₅₀. Therefore, when the fraction inhibition is >80%, we measured the inhibition at 30 μM compound concentration and fit to the equation:

$$\% \text{ inhibition} = 100 \frac{[\text{inhibitor}]}{[\text{inhibitor}] + IC_{50}}.$$

Kinetics of Recovery of Inhibition from M2WJ332 Inhibition. To probe the rate of dissociation of M2WJ332, a washout experiment was carried out in our electrophysiological assay (Fig. S2). An oocyte expressing S31N was incubated with 100 μM M2WJ332 to achieve complete inhibition, and the bathing solution was then switched to drug-free pH 5.5 Barth's solution for 20 min to determine the channel activity recovery. The recovery of the channel activity was very slow compared with the recovery of amantadine inhibition on the A/M2-S31N channel (1).

Plaque Reduction Assay at 50 μM Compound Concentration Against A/WSN/33. Plaque reduction assay of selected compounds at 50 μM is shown in Fig. S3.

NMR Samples Preparation. Deuterated n-dodecylphosphocholine (DPC) (Cambridge isotope) powder was weighed using a microbalance; peptide and drug were added to the powder from their ethanol stocks with the desired molar ratio. The mixture was vortexed, and the ethanol was removed by nitrogen purging; the residue was subsequently left on a lyophilizer overnight to remove ethanol completely. Buffer [10% D₂O in H₂O, 50 mM NaPi (pH 6.8)] was added to the dried mixture and vortexed for 2 min. The final pH was adjusted to 6.8 with NaOH or H₃PO₄. The final NMR sample condition is 2 mM A/M2-S31N (19–49) (monomer), 20 mM M2WJ332, 100 mM deuterated DPC (Cambridge isotope), and 50 mM sodium phosphate buffer (pH 6.8).

NMR Spectroscopy. All 1D, 2D, or 3D spectra were recorded with standard pulse sequences (2, 3). Here, we only list the parameters for the 150-ms NOESY spectra that were used for structure determination. The 2D ¹⁵N-(¹H)-¹H NOESY experiment for the ²H-¹⁵N sample was carried out with $t_{1,\text{max}} = 59$ ms and $t_{2,\text{max}} = 81$ ms (16 scans). The 2D ¹³C-(¹H)-¹H NOESY experiments for selectively labeled peptides were carried out with $t_{1,\text{max}} = 7$ ms and $t_{2,\text{max}} = 71$ ms (128 scans). The 3D ¹³C-edited NOESY experiments were carried out for VANIG, VGIHL, and ¹³C-¹⁵N uniformly labeled samples (a description of these samples is provided below) with $t_{1,\text{max}}(^1\text{H}) = 11$ ms, $t_{2,\text{max}}(^{13}\text{C}) = 4.4$ ms, and $t_{3,\text{max}}(^1\text{H}) = 80$ ms

(8 scans). The 3D ¹⁵N-edited NOESY experiments were carried out for ¹³C-¹⁵N and ²H-¹⁵N uniformly labeled samples with $t_{1,\text{max}}(^1\text{H}) = 11$ ms, $t_{2,\text{max}}(^{15}\text{N}) = 21$ ms, and $t_{3,\text{max}}(^1\text{H}) = 70$ ms (16 scans). Two 3D ¹³C-edited and ¹³C-¹⁵N-filtered NOESY spectra were recorded for a ¹³C-¹⁵N sample to detect protein–drug intermolecular NOEs, and a mixture of 50% unlabeled and 50% ¹³C-¹⁵N uniformly labeled sample was tested to detect interhelical NOEs, with $t_{1,\text{max}}(^1\text{H}) = 11$ ms, $t_{2,\text{max}}(^{13}\text{C}) = 4.2$ ms, and $t_{3,\text{max}}(^1\text{H}) = 70$ ms (16 scans). The ¹H carrier frequency was always set to the water signal, and chemical shifts were referenced with respect to the residual water peak at 4.63 ppm. All spectra were processed and analyzed using the NMRPipe program (4). The first one-third of time domain data in the indirect ¹³C or ¹⁵N dimensions was extended by linear prediction. Time domain data were multiplied by sine square bell window functions shifted by 90° and zero-filled once before Fourier transformation. Spectra were analyzed with the XEASY (5).

Sequence-specific backbone (¹H^N, ¹⁵N, and ¹³C^α) and ¹³C^β resonance assignments were obtained using 3D TROSY-based HNCA and HN(CA)CB recorded on the ²H-¹³C-¹⁵N sample and confirmed by 3D ¹⁵N NOESY for the characteristic sequential ¹H^N-¹H^N NOEs. Assignments were then extended to side chains by 3D CCH-TOCSY and ¹³C NOESY for the ¹³C-¹⁵N uniformly labeled sample and by 2D C(C)H-TOCSY and ¹³C-(¹H)-¹H NOESY for specifically labeled samples. Furthermore, stereospecific assignments for isopropyl groups of Val and Leu were obtained with the 10% fractionally ¹³C-labeled samples (6).

Structure Calculations. ¹H-¹H distance constraints for structure calculations were extracted from NOESY spectra (Fig. S7C). For nondeuterated samples, NOE cross-peaks were classified as strong (1.8–3.5 Å), medium (1.8–4.0 Å), weak (1.8–5.0 Å), and very weak (1.8–5.5 Å) by referencing to the NOE intensities observed for protons of fixed distances (e.g., geminal methylene protons or vicinal protons in aromatic rings). For deuterated samples, NOE cross-peaks were classified as strong (1.8–5.0 Å), medium (1.8–5.5 Å), weak (1.8–7.0 Å), and very weak (1.8–8.0 Å) by referencing to the NOE intensities observed for sequential ¹HN-¹HN in helices. To prevent overconstrained NOEs, conservative upper bound distances were generally applied, especially for the weak or partially overlapped peaks. The lower bound is set as 1.8 Å for all distance constraints. Backbone dihedral angle constraints were derived from chemical shifts using the program TALOS+ (7). Based on ¹³C chemical shifts, strong sequential ¹HN-¹HN NOEs, and Phi/Psi torsional angles predicted by TALOS+, we identified residues 26–44 to be a regular α-helix; thus, we added hydrogen bond restraints to that portion. Moreover, to take the unusual proton chemical shift of His37 HE1 (4.92 ppm) into consideration, which is the second most upfield-shifted proton in the entire BioMagResBank database for nonparamagnetic protein (8), six artificial distances were added between the His37 HE1 and W41 indole ring in addition to the “1H shifts” module in Xplor-NIH. With the input of all mentioned restraints, the structure was calculated by simulated annealing in torsion angle space using the Xplor-NIH program by slowly cooling an extended structure from 3,000 K to 20 K. The final parameters for target function are 1,000 kcal·mol⁻¹·Å⁻² for bond lengths; 500 kcal·mol⁻¹·rad⁻² for angles and improper dihedrals; 4 kcal·mol⁻¹·Å⁻⁴ for the quartic van der Waals repulsion term; 30 kcal·mol⁻¹·Å⁻² for distance restraints, including the NOE and hydrogen bond; and 200 kcal·mol⁻¹·rad⁻² for dihedral angle restraints. A family of 20 of the lowest energy structures was selected from 100 calculated structures to represent the solution structure.

Comparison of amide chemical shifts between S31N–M2WJ332 and WT–M2WJ10 complexes shows that the average differences are ~0.25 ppm and ~0.05 ppm for the N- and C-terminal parts, respectively, and that His37 is on the separation line (Fig. S4A). In addition, TROSY heteronuclear single quantum coherence (HSQC) peaks of 24–33 are quite weak for S31N (Fig. 3B). These observations could be due to S31N mutation, as well as to the drug

position. We also compared the ^{13}C chemical shifts of the S31N–drug complex with the corresponding chemical shifts of two conformationally distinct conformers seen in the solid-state NMR of S31N in lipid bilayers (9). Only one of the two conformers has a good correlation ($R^2 = 0.88$) with the major conformer that was observed in the present study (Fig. S4B). The other conformation seen in the solid state might be similar to that of a second conformer we observed at lower and higher pH (Fig. S4B).

The ^{15}N HSQC spectra were recorded in presence of **M2WJ332** at different pHs to identify the optimal condition (Fig. S4C). The chemical shift of indole NH of W41 is sensitive to aromatic packing, and the peak at ~ 11.2 ppm, which was seen in the pH 6.8 form, was strongly shifted from this residue's intrinsic chemical shift and indicative of tight packing of the Trp41/His37 tetrads in the structure of the complex. At lower and higher pH, an increased population of an indole NH peak at ~ 10.4 ppm, which is close to this residue's intrinsic chemical shift, was seen. This finding suggested that the C-terminal region is either less tightly packed and/or more dynamic; hence, it is labeled the “open form” in Fig. S4D, showing the population as a function of pH. It is clear that in presence of the drug, the S31N has a narrow pH window, where it takes the compact “closed form.”

To detect NOEs between amide protons and the drug, the NOESY spectrum was taken for a uniformly ^{15}N - ^2H -labeled A/M2-S31N (19–49) with **M2WJ332** in the DPC micelle at pH 6.8 (Fig. S5C). We obtained assignments for the drug dissolved in the exact same sample conditions but in the absence of peptide (Fig. S64). The right half of the spectrum in Fig. S5C, where only intermolecular NOEs appear, showed that the adamantyl ring interacted with the amides from residue I32 to H37. Strong NOE cross-peaks were observed between H6, H7, and H8 from the adamantyl ring of the drug and the G34 amide. H6 from the drug also interacts with I32 and H37 amides, and weak NOE cross-peaks were seen between H7 and H8 from the drug and I35 and H37 amides, respectively. These NOEs shows that the drug binds to the M2 channel with its aromatic headgroup facing the N-terminal lumen.

To determine this binding orientation clearly, three peptides with the particular residues ^{15}N and ^{13}C selectively labeled were synthesized, and 2D or 3D ^{13}C -edited NOESY was recorded with **M2WJ332** under the identical buffer and experimental conditions. The first is with residues at the N-terminal lumen V27, A30, N31, I33, and G34 ^{15}N and ^{13}C selectively labeled (refer to VANIG peptide afterward); the second is with residues at the C-terminal of the channel G34, I35, H37, and L38 ^{15}N and ^{13}C electively labeled (refer to VGIHL peptide afterward); and the last is with residues L26, A29, G34, I42 and F47 ^{15}N and ^{13}C electively labeled (refer to LAGIF peptide afterward). The first two peptides were designed to incorporate all channel-facing residues, such as V27, A30, N31, G34, and H37; in addition, all labeled residues in each residue are unique, such that chemical shift assignment, as well as NOE assignment, is straightforward and unambiguous in most cases. The third peptide was used as a control. Helix interface-facing residues, such as V28, I33, I35, and L38, were also included in the designed peptides. As an internal control of sample reconstitution, G34 was incorporated into both peptides. Strong NOE cross-peaks were observed in the VANIG spectra showing that H1, H2, and H3 from the thiophene ring interact with γ_1 and γ_2 methyls of V27; similar strong NOE peaks were also found between H4 from the isoxazole ring and γ_1 and γ_2 methyls of V27 (Fig. 2B and Figs. S6 and S7). No NOE cross-peaks were detected between the aromatic headgroup protons from the drug and residues after A30 (Fig. S5E), which validated the hypothesis that drug binds to the channel with the aromatic headgroup facing up to the N-terminal lumen. To compare NOEs directly, mixing time for all NOESY spectra were set as 150 ms. To confirm that the NOE cross-peaks seen from the ^{13}C -edited NOESY are not from spin diffusion, some 2D or 3D NOESY spectra were repeated at different mixing times of 75 ms or 100 ms.

Molecular Dynamics Simulations. The lead compound **M2WJ332** was simulated in complex with the WT (Udorn) transmembrane (TM; 25–46) domain of influenza A virus M2 proton channel (M2TM) and its S31N mutant until its pose within each protein pore was converged (about 80 ns of simulated time). The sequences of the peptides are PLVVAASIIGILHLILWILDRL and PLVVAANIIGILHLILWILDRL for WT and S31N mutant, respectively. The sequence of the full-length M2 is provided in the study by Kochendoerfer et al. (10). When initialized with its aromatic headgroup directed toward H37 and its adamantine group arranged like that of amantadine in WT-M2TM, **M2WJ332** moved away from its initial position, finding a new equilibrium arrangement with its secondary amine closer to residue 31. When initialized with its aromatic headgroup toward the viral exterior, the drug reached equilibrium with its amine at the same position described above, with comparatively lower fluctuations. In Fig. S84, we show the final structure of **M2WJ332** in complex with S31N-M2TM: The drug molecule is involved in a network of H-bonds with N31, sharing two immobilized water molecules. The arrangement with the aromatic headgroup pointing toward the exterior (Fig. S8 A and C) also fits best the measured solution NMR signals: Short distances between the drug and residues V27 and A30 are compatible with the measured strong ^1H - ^1H NOE signals (Fig. S8C). Because the time scales necessary to observe drug release are much longer (microseconds to milliseconds), our calculations only describe the local features of their drug–M2TM interactions rather than the absolute binding affinities. However, the variance of the amine position in all directions (Δr^2) is systematically larger than threefold the variance along the channel's axis only (Δz^2) (Fig. S8D). This indicates that the drug favors motions along the pore axis. This effect is particularly significant in the complex with S31N-M2TM, where the axial variance (Δz^2) is 1/13th of the total variance (Δr^2). This correlates very well with the much higher activity against S31N-M2TM than the other mutants.

The NMR structure of A/M2-S31N (19–49) and **M2WJ332** solved by NMR was also embedded in the same hydrated bilayer. In addition to the above protocol, we applied the NOE distance restraints used for the NMR structure calculation. The force constant of the restraints was initially set at the final value of the NMR structure calculation ($30 \text{ kcal}\cdot\text{mol}^{-1}\cdot\text{\AA}^2$) and gradually decreased to $2 \text{ kcal}\cdot\text{mol}^{-1}\cdot\text{\AA}^2$ over 20 ns of simulated time. During the initial minimization, the Asn31 side chains (not restrained by any NOE signal) moved from the initial $\chi_1 \sim -70^\circ$ to $\chi_1 \sim -60^\circ$, so as to form H-bonds with water molecules outside the pore. As the distribution of water molecules throughout the pore reached equilibrium, the Asn31 side chains formed the same pattern of water-mediated H-bonds with the **M2WJ332** aromatic headgroup. The χ_2 angle of each Asn31 underwent high dynamics between the minimization and the first nanosecond of restrained dynamics, only to stabilize to a final configuration like that observed in the unrestrained molecular dynamics (MD) ($\chi_2 \sim -25^\circ$). No major conformational changes were observed in the backbone structure of the bundle, with the exception of the recovery of an α -helical structure closer to ideal. Specifically, the 32–36 backbone H-bond distance, which was elongated at 3.2 \AA in the NMR structure, decreased to the usual 2.9 \AA during the MD simulation. In Fig. S8E, we report the rmsd with respect to the NMR structure during the final stages of (i) the simulation of S31N-M2TM (25–46) modeled after the X-ray structure of WT-M2TM (25–46) and without external forces or experimental bias and (ii) the simulation of S31N-M2TM (19–49) initialized from the NMR structure and simulated with soft restraints to reproduce the NOE-measured distances. The backbone rmsds with respect to the NMR structure have the typical amplitude associated with thermal motions for this protein ($\sim 1 \text{ \AA}$). In particular, the rmsd of the drug-binding segment (25–34) is low in both simulations, indicating that the interactions between M2 and the **M2WJ332** molecule are well determined by our computational protocol and can be observed both with and without experimental restraints.

- Jing X, et al. (2008) Functional studies indicate amantadine binds to the pore of the influenza A virus M2 proton-selective ion channel. *Proc Natl Acad Sci USA* 105(31):10967–10972.
- Cavanagh J, Fairbrother WJ, III, Rance M, Skelton NJ (2007) *Protein NMR Spectroscopy: Principles and Practice* (Academic, Amsterdam, Boston).
- Sattler M, Schleucher J, Griesinger C, Smith ME, Eck ERHv (1999) *Heteronuclear Multidimensional NMR Experiments for the Structure Determination of Proteins in Solution Employing Pulsed Field Gradients* (Elsevier, Amsterdam).
- Delaglio F, et al. (1995) NMRPipe: A multidimensional spectral processing system based on UNIX pipes. *J Biomol NMR* 6(3):277–293.
- Bartels C, Xia TH, Billeter M, Güntert P, Wüthrich K (1995) The program XEASY for computer-supported NMR spectral analysis of biological macromolecules. *J Biomol NMR* 6(1):1–10.
- Neri D, Szyperki T, Otting G, Senn H, Wüthrich K (1989) Stereospecific nuclear magnetic resonance assignments of the methyl groups of valine and leucine in the DNA-binding domain of the 434 repressor by biosynthetically directed fractional ¹³C labeling. *Biochemistry* 28(19):7510–7516.
- Shen Y, Delaglio F, Cornilescu G, Bax A (2009) TALOS+: A hybrid method for predicting protein backbone torsion angles from NMR chemical shifts. *J Biomol NMR* 44(4):213–223.
- Ulrich EL, et al. (2008) BioMagResBank. *Nucleic Acids Res* 36(Database issue): D402–D408.
- Andreas LB, Eddy MT, Chou JJ, Griffin RG (2012) Magic-angle-spinning NMR of the drug resistant S31N M2 proton transporter from influenza A. *J Am Chem Soc* 134(17): 7215–7218.
- Kochendoerfer GG, et al. (1999) Total chemical synthesis of the integral membrane protein influenza A virus M2: Role of its C-terminal domain in tetramer assembly. *Biochemistry* 38(37):11905–11913.

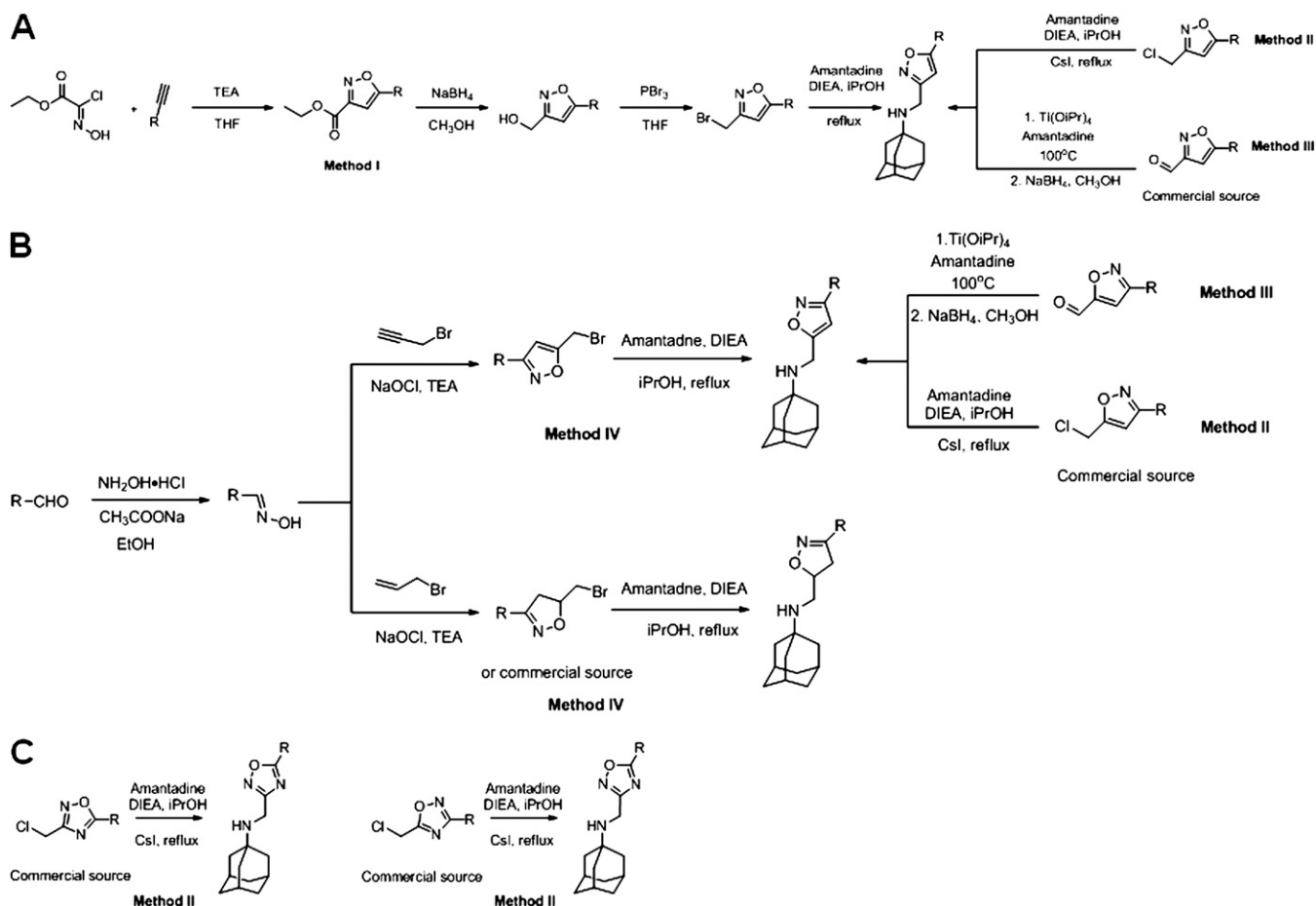


Fig. S1. Synthesis schemes of compounds with isoxazole (A and B), isoxazoline (B) and 1,2,4-oxadiazole (C) headgroups. The isoxazole and isoxazoline compounds were synthesized by [3 + 2] cyclization starting from in situ-generated nitrone reacting with alkyne or alkene. DIEA, N,N-Diisopropylethylamine; TEA, triethylamine.

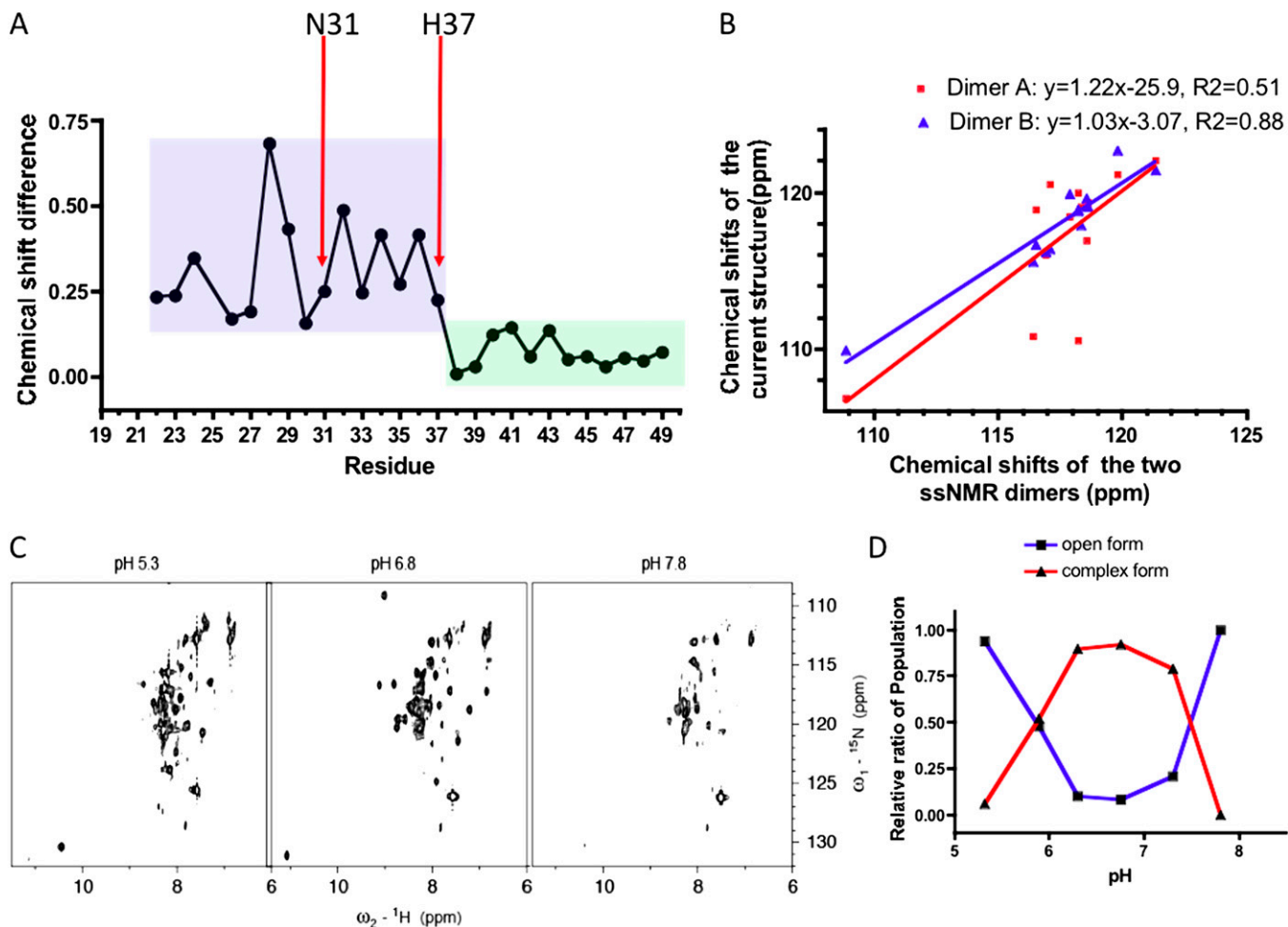


Fig. S4. (A) Chemical shift difference as a function of residue number between WT-M2TM (19–49) WT in the presence of M2WJ10 (1) at pH 7.5 and S31N in the presence of M2WJ322 at pH 6.8. Chemical shift differences were calculated using $\Delta\delta = [1/2((\Delta\delta^1\text{H})^2 + (1/5\Delta\delta^{15}\text{N})^2)]^{1/2}$. (B) Correlation plots of ^{15}N chemical shifts for residues 26–42 between the current solution NMR structure and the two dimers obtained by solid-state NMR (ssNMR) (2). (C) ^{15}N HSQC spectra in presence of M2WJ332 at pH 5.3, 5.9, 6.3, 6.8, 7.3, and 7.8 on a Bruker 800-MHz spectrometer. (D) Populations of open and complex forms as a function of pH. Population was calculated as a ratio of the peak volume to the sum of the two peak volumes for each pH step.

1. Cady SD, Wang J, Wu Y, DeGrado WF, Hong M (2011) Specific binding of adamantane drugs and direction of their polar amines in the pore of the influenza M2 transmembrane domain in lipid bilayers and dodecylphosphocholine micelles determined by NMR spectroscopy. *J Am Chem Soc* 133(12):4274–4284.
2. Andreas LB, Eddy MT, Chou JJ, Griffin RG (2012) Magic-angle-spinning NMR of the drug resistant S31N M2 proton transporter from influenza A. *J Am Chem Soc* 134(17):7215–7218.

A

1 2KQT (Hong, SSnmr)
 2 2L0J (Cross, SSnmr)
 3 2RLF (Chou, Solution nmr)
 4 3C9J (DeGrado, Xray)
 5 3LBW (DeGrado, Xray)
 6 S31N (DeGrado, Solution nmr)

RMSD table:

	1	2	3	4	5	6
1		0.92	1.28	2.91	0.73	0.67
2	0.92		1.69	2.54	0.86	1.32
3	1.28	1.69		3.62	1.57	1.14
4	2.91	2.54	3.62		2.96	2.94
5	0.73	0.86	1.57	2.96		1.27
6	0.67	1.32	1.14	2.94	1.27	

mean global RMSD: 1.76 +/- 0.97 Å (0.67.. 3.62 Å)

average RMSD of each structure to the rest:

structure 1 : 1.30 +/- 0.93 Å (0.67.. 2.91 Å)
 structure 2 : 1.47 +/- 0.69 Å (0.86.. 2.54 Å)
 structure 3 : 1.86 +/- 1.01 Å (1.14.. 3.62 Å)
 structure 4 : 2.99 +/- 0.39 Å (2.54.. 3.62 Å)
 structure 5 : 1.48 +/- 0.89 Å (0.73.. 2.96 Å)
 structure 6 : 1.47 +/- 0.86 Å (0.67.. 2.94 Å)

B



C

S31N	
NMR distance and dihedral constraints	
per monomer	
Total NOE	215
Protein-drug	23
Inter-helical	28
Intra-helical	164
Intra-residue	100
Sequential (i-j = 1)	40
Medium-range (i-j < 4)	24
Long-range (i-j > 5)	0
phi	20
psi	20
Structure statistics	
Violations (mean and s.d.)	
Distance constraints (>0.5 Å)	0
Dihedral angle constraints (>5°)	0
rmsd to the mean structure residue 26-45 (Å)	
Heavy	0.47±0.19
Backbone	1.15±0.21

Fig. S7. Comparison of six different M2 structures. (A) Rmsds among different M2 structures (1–4). The rmsds of the S31N structure is highlighted in blue. (B) Backbone rmsd as a function of residue number among the six structures (S31N, 2KQT, 2L0J, 2RLF, 3C9J, and 3LBW). (C) NMR and refinement statistics for the solution structure.

- Hong, Cady SD, et al. (2010) Structure of the amantadine binding site of influenza M2 proton channels in lipid bilayers. *Nature* 463(7281):689–692.
- Cross, Sharma M, et al. (2010) Insight into the mechanism of the Influenza A proton channel from a structure in a lipid bilayer. *Science* 330(6003):509–512.
- Chou, Schnell JR, Chou JJ (2008) Structure and mechanism of the M2 proton channel of influenza A virus. *Nature* 451(7178):591–595.
- DeGrado, Stouffer AL, et al. (2008) Structural basis for the function and inhibition of an influenza virus proton channel. *Nature* 451(7178):596–599.
- DeGrado, Acharya R, et al. (2010) Structure and mechanism of proton transport through the transmembrane tetrameric M2 protein bundle of the influenza A virus. *Proc Natl Acad Sci USA* 107(34):15075–15080.
- DeGrado. Current study.

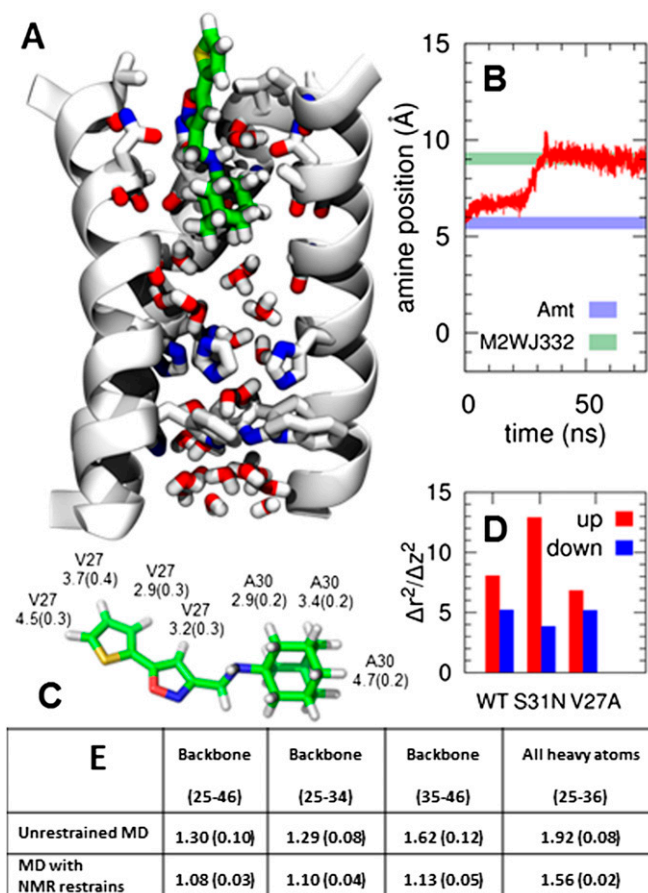


Fig. S8. (A) Structure of the complex between S31N-M2TM and M2WJ332 after 80 ns of MD simulation. The protein is shown as a cartoon, with the V27, N31, A30, H3,7 and W41 as sticks. The drug is shown in green, surrounded by water molecules throughout the pore. Water between N31 and G24, although present in the initial stages, was absent through the second half of the MD run. (B) Time evolution of the amine's position (red) along the channel axis: The two bands corresponding to this simulation (light green) and one with amantadine bound to WT-M2TM (light blue) are shown for comparison. (C) Average H-H distances between the drug and the pore residues, computed as averages of $1/r^6$ across chemically equivalent hydrogens (SDs are shown in parentheses). (D) Ratios between the variance of the amine position in all directions (Δr^2) and along the channel axis only (Δz^2) for the two mutants and the two initial orientations of the drug. (E) Rmsds in angstrom from the NMR structure of S31N-M2TM in complex with M2WJ332, with two different protocols: (i) unbiased MD simulation, initialized from a model of S31N based on the X-ray structure of WT-S31N, and (ii) MD refinement of the NMR structure, with soft NOE restraints.

Table S1. Structure-activity relationship of isoxazole-, 1,2,4-oxadiazole-, and isoxazoline-containing compounds

	R	X	ID	S31N*	WT*	IC ₅₀ [†] , μM
		C	M2WJ367	65/N.T.	5	54
		C	M2WJ370	44/N.T.	14	125
		C	M2WJ368	80/52	4	27
		N	M2WJ393	71/N.T.	7	42
		C	M2WJ371	8/N.T.	14	1,070
		N	M2WJ434	62/N.T.	21	62
		C	M2WJ446	25/N.T.	14	293
		N	M2WJ397	43/N.T.	14	131
		N	M2WJ398	52/N.T.	6	92
		N	M2WJ430	20/N.T.	11	403
		N	M2WJ423	42/N.T.	4	140
		C	M2WJ380	48/N.T.	10	110
		N	M2WJ381	32/N.T.	0	208
		N	M2WJ377	19/N.T.	10	435
		C	M2WJ361	16/N.T.	16	514

N.T., not tested; R, substitutions; X, C or N.

*Values represent the mean of three independent measurements. We typically see no more than 5% variation in the percent of inhibition on a given day, or 10% error for measurements made on different days with different batches of oocytes. All compounds were initially tested at 100 μM. Compounds that showed greater than 80% inhibition at 100 μM were further tested at 30 μM. The data are presented as the percent (%) of inhibition at 100 μM/% inhibition at 30 μM.

[†]S31N IC₅₀s were calculated based on the equation derived from nonlinear regression curve fitting of a set of compounds with experimentally measured IC₅₀s and percent of inhibition at 100 μM (Fig. S2).